HHS Public Access

Author manuscript

Exp Eye Res. Author manuscript; available in PMC 2022 September 01.

Published in final edited form as:

Exp Eye Res. 2021 September ; 210: 108715. doi:10.1016/j.exer.2021.108715.

Characterization and allogeneic transplantation of a novel transgenic cone-rich donor mouse line

Ying V. Liu[a], **Derek Teng**[a], **Gregory J. Konar**[a], **Dzhalal Agakishiev**[a], **Alexis Biggs-Garcia**[a], **Sarah Harris-Bookman**[a], **Minda M. McNally**[a], **Catalina Garzon**[a], **Saalini Sastry**[b], **Mandeep S. Singh**[a,*]

[a]Wilmer Eye Institute, Johns Hopkins University School of Medicine, Baltimore, MD, USA

[b]Zanvyl Krieger School of Arts and Sciences, Johns Hopkins University, Baltimore, MD, USA

Abstract

Objectives: Cone photoreceptor transplantation is a potential treatment for macular diseases. The optimal conditions for cone transplantation are poorly understood, partly because of the scarcity of cones in donor mice. To facilitate allogeneic cone photoreceptor transplantation studies in mice, we aimed to create and characterize a donor mouse model containing a cone-rich retina with a cone-specific enhanced green fluorescent protein (EGFP) reporter.

Methods: We generated *OPN1LW-EGFP/NRL*$^{-/-}$ mice by crossing *NRL*$^{-/-}$ and *OPN1LW-EGFP* mice. We characterized the anatomical phenotype of *OPN1LW-EGFP/NRL*$^{-/-}$ mice using multimodal confocal scanning laser ophthalmoscopy (cSLO) imaging, immunohistology, and transmission electron microscopy. We evaluated retinal function using electroretinogram (ERG), including 465 and 525 nm chromatic stimuli. Retinal sheets and cell suspensions from *OPN1LW-EGFP/NRL*$^{-/-}$ mice were transplanted subretinally into immunodeficient *Rd1* mice.

Results: *OPN1LW-EGFP/NRL*$^{-/-}$ retinas were enriched with OPN1LW-EGFP^{+} and S-opsin^{+} cone photoreceptors in a dorsal-ventral distribution gradient. Cone photoreceptors co-expressing OPNL1W-EGFP and S-opsin significantly increased in *OPN1LW-EGFP/NRL*$^{-/-}$ compared to *OPN1LW-EGFP* mice. Temporal dynamics of rosette formation in the *OPN1LW-EGFP/NRL*$^{-/-}$ were similar as the *NRL*$^{-/-}$ with peak formation at P15. Rosettes formed preferentially in the ventral retina. The outer retina in P35 *OPN1LW-EGFP/NRL*$^{-/-}$ was thinner than *NRL*$^{-/-}$ controls. The *OPN1LW-EGFP/NRL*$^{-/-}$ ERG response amplitudes to 465 nm stimulation were similar to, but to 535 nm stimulation were lower than, *NRL*$^{-/-}$ controls. Three months after transplantation, the suspension grafts showed greater macroscopic degradation than sheet grafts. Retinal sheet grafts from *OPN1LW-EGFP/NRL*$^{-/-}$ mice showed greater S-opsin+ cone survival than suspension grafts from the same strain.

[*]**Corresponding author:** Mandeep S. Singh, Address: Wilmer Eye Institute, Johns Hopkins University School of Medicine, 600 N. Wolfe St, Baltimore, MD 21287, USA, mandeep@jhmi.edu.

Declarations of interest:
None

Conclusions: *OPN1LW-EGFP/NRL*$^{-/-}$ retinae were enriched with S-opsin^{+} photoreceptors. Sustained expression of EGFP facilitated the longitudinal tracking of transplanted donor cells. Transplantation of cone-rich retinal grafts harvested prior to peak rosette formation survived and differentiated into cone photoreceptor subtypes. Photoreceptor sheet transplantation may promote greater macroscopic graft integrity and S-opsin^{+} cone survival than cell suspension transplantation, although the mechanism underlying this observation is unclear at present. This novel cone-rich reporter mouse strain may be useful to study the influence of graft structure on cone survival.

Keywords

Degenerative retinal diseases; age-related macular degeneration; stem cell therapy; cone photoreceptor; cone transplantation; optic coherence tomography

1. Introduction

Cone photoreceptors mediate central vision in humans, including high-acuity and color vision. Degenerative retinal diseases, such as age-related macular degeneration (AMD) (Curcio et al., 1996; Shelley et al., 2009), Stargardt disease (Chen et al., 2011; Yzer et al., 2007), retinitis pigmentosa (RP) (Li et al., 2015; Makiyama et al., 2013; Sobaci et al., 2012), and achromatopsia (Chang et al., 2006; Hurlbert et al., 1998; Thiadens et al., 2010) can cause irreversible loss of cone photoreceptors and result in loss of color vision, and blindness. There is an unmet need to develop methods to regenerate or replace cone photoreceptors, as treatments for these conditions.

Photoreceptor transplantation is a promising approach, given its potential to reconstitute the structure and function of the degenerate retina (Homma et al., 2013; Reh, 2016; Singh et al., 2013). Rod photoreceptor transplantation has been studied in depth (MacLaren et al., 2006), and several important studies have shown optimized protocols to induce rod-dominant retinal organoids from pluripotent stem cells (Brooks et al., 2019; Chichagova et al., 2019; Mandai et al., 2017; Zhong et al., 2014). In contrast, there is a relative lack of information on the optimal methods for successful cone photoreceptor regeneration (Eldred et al., 2018; Kim et al., 2019). This is partly because of the scarcity of donor cone photoreceptors for experimentation in wild-type mice. There are 30 times fewer cones than rods in the murine retina (Chichagova et al., 2019), limiting the number of donor cells that can be harvested per animal, and necessitating purification methods that can be damaging to the cells. Thus, an appropriate cone-rich donor mouse model would facilitate further research on cone transplantation. Cone photoreceptor transplantation holds clinical relevance in terms of therapy for not only the primary cone degeneration and dysfunction syndromes, but also in RP where cone loss is a consequence of primary rod loss.

Deletion of the neural retina leucine (*NRL*) gene results in the enrichment of cone-like photoreceptors in mice (Mears et al., 2001). The *NRL*$^{-/-}$ mice model is well-established, but the lack of an endogenous cone-specific fluorescent reporter limits its application for *in vivo* transplantation research (Akimoto et al., 2006; Samson et al., 2009), wherein donor cell tracing is a priority. The strategy of ubiquitously expressing green fluorescent protein (GFP) in *NRL*$^{-/-}$ mice necessitated the purification of donor cones by CD73-based

magnetic-activated cell sorting (MACS), which was found to be relatively inefficient due to low CD73 expression in primary cone photoreceptors (Santos-Ferreira et al., 2015). Another reported approach relied on genetic trapping of the *Ccdc136-GFP* allele, that induces GFP expression in both L/M- and S-opsin expressing cones. The purification of the GFP^+ cone photoreceptors is possible in *CCDC136-GFP/NRL*$^{-/-}$ mice because the GFP is limited to cone cells before P14. However, in experiments that prioritize the use of non-sorted donor cell transplantations (for example, for cell viability concerns), the eventual expression of CCDC136-GFP in rod bipolar cells after P14 may confound cone-specific quantification in recipients without additional immunolabeling (Smiley et al., 2016a and 2016b). These studies underscore the significance of ongoing efforts to develop cone photoreceptor reporter models for transplantation research and highlight the challenges of introducing fluorescent reporters in cone-rich mice.

Here, our goal was to facilitate allogeneic cone transplantation studies in rodent models by characterizing a novel donor strain containing a cone-rich retina and a cone-specific enhanced green fluorescent protein (EGFP) reporter. We leveraged the *OPN1LW-EGFP* mouse developed by Fei *et al.* (Fei and Hughes, 2001), in which human *OPN1LW* promoter-driven *EGFP* expression is restricted to a subset of mouse cones. We created a novel transgenic mouse model (*OPN1LW-EGFP/NRL*$^{-/-}$) by crossing the *NRL*$^{-/-}$ and the *OPN1LW-EGFP* lines. We aimed to study the density distribution of EGFP tagged cone photoreceptors in this model, focusing on whether the addition of *OPN1LW-EGFP* would alter the reported *NRL*$^{-/-}$ phenotype in structural and functional terms. Specifically, we hypothesized that the temporal dynamics of rosette formation in the *OPN1LW-EGFP/NRL*$^{-/-}$ retina is the same as in *NRL*$^{-/-}$. Furthermore, we sought to understand photoreceptor rosette development in *OPN1LW-EGFP/NRL*$^{-/-}$ mice in detail, as this is a known feature in the *NRL*$^{-/-}$ line that has the potential to influence the efficiency of regeneration after transplantation. We also aimed to explore the utility of donor *OPN1LW-EGFP/NRL*$^{-/-}$ photoreceptors for cone photoreceptor allotransplantation in retinal-degenerate recipients. In this regard, we hypothesized that transplantation of donor cones harvested prior to peak rosette formation will survive and mature in the recipient. Recognizing that pre-formed laminar sheet transplantation may promote photoreceptor cell alignment and polarity, we included a comparison of sheet and suspension transplants.

2. Methods & Materials

2.1 Animals

All animal experiments were carried out according to the National institutes of Health guide for the care and use of Laboratory animals (NIH Publications No. 8023, revised 1978) and ARVO Statement for the Use of Animals in Ophthalmic and Vision Research. All procedures were approved by the Johns Hopkins University Animal Care and Use Committee (M016M17). The C57/BL6J (wild-type, *WT*), *NRL*$^{-/-}$, *OPN1LW-EGFP*, *C3H/HeJ-Pde6brd1* (referred to as *rd1*), and *NOD.CB17-Prkdcscid/J* (referred to as *NS*) mice of either gender (aged 6 to 8 weeks) were obtained from Jackson Laboratory (USA). All mice were housed in cages under a 12:12-hour light-dark cycle with water and food provided *ad libitum*.

2.2 Breeding and Genotyping

The breeding strategy was performed as previously reported (Wenzel et al., 2007). The *OPN1LW-EGFP/NRL*$^{-/-}$ mice were created by an outcross of homozygous *NRL*$^{-/-}$ and *OPN1LW-EGFP* mice (aged 8 weeks). Recipient *C3H/HeJ-Pde6brd;NOD.CB17-Prkdcscid/J* double-mutant mice (referred to as *Rd1/NS)* were created by crossing homozygous *rd1* and *NOD/SCID* mice (aged 8 weeks). Genomic DNA of the third-generation offspring was extracted from ear biopsies and genotyped by Transnetyx Tag Center (Cordova, USA). Primers were listed in Supplementary Table S1. The homozygous offspring were selected for the following experiments.

2.3 Retinal flat-mount staining and quantification

OPN1LW-EGFP/*NRL*$^{-/-}$, *OPN1LW-EGFP*, *NRL*$^{-/-}$, and *WT* mice aged P36-P45 (n=10 eyes/strain) were sacrificed and heart-perfused with 4% paraformaldehyde (PFA) in phosphate-buffered saline (PBS) (Electron Microscopy Sciences, Hatfield, PA, USA). Neural retinal cups were gently isolated as reported (Singh et al., 2013) and fixed in 2% PFA/PBS for 30 minutes (min) at room temperature (RT). Retina cups were rinsed with PBS (5 min × 3), then blocked with 10% goat serum and permeabilized with 0.5% Triton-X100 at 4°C overnight. After PBS rinse (10 min × 3), retinal cups were incubated with primary antibody at 4°C overnight and rinsed in PBS at RT (1hour × 4). Following the rinse, retinal cups were incubated with secondary antibody overnight at 4°C, rinsed in PBS (1hour × 4) and counterstained nuclear with 4′,6-diamidino-2-phenylindole (DAPI) (Sigma-Aldrich, St. Louis, USA) (1:1000, 30 min, RT). Primary and secondary antibodies used are listed in Table S2. Stained retinal cups were rinsed in PBS (10 min × 3) and flattened using four cuts from the periphery toward the center, then mounted with ProLong Diamond mounting media (Life Technology, NY, USA). Twelve equally distributed regions, from the peripheral to the central retina, per flat mount were imaged with a confocal laser scanning microscope (LSM 510, Zeiss, USA). Fluorescent signal density was automatically measured using ImageJ. The density percentage equaled the numerical ratio of fluorescent area to total imaged area. Three-dimensional rosettes were reconstituted using Z-stacks projection in Imaris software (Version 9.5.0, Bitplane AG, Zurich, Switzerland).

2.4 Transplantation

Retinal sheets or cell suspension were obtained from the whole *OPN1LW-EGFP/NRL*$^{-/-}$ retina (P6) as previously reported (Liu et al., 2020). To obtain retinal sheet, the cornea, lens, and vitreous cavity were removed, the neural retina was gently isolated and suspended in sterile HBSS, and were cut into 1 × 2 mm^2 sheets (hereinafter referred to as ‘sheets’) using 27-gauge (G) horizontal curved scissors (VitreQ, USA) under a dissection microscope. To obtain retinal cell suspension, the neural retina was dissociated into single cell suspension using Papain Kit (Papain Dissociation System, Worthington Biochemical, USA). Living cells were resuspended in HBSS at a density of 2×10$^{\wedge 5}$ cells/μl. *Rd1/NS* mice recipients (aged 8 weeks, n= 8 eyes) were anesthetized with ketamine (100 mg/kg body weight) and xylazine hydrochloride (20 mg/kg body weight). Pupils were dilated with 1% (WT/vol) tropicamide (Bausch & Lomb, USA). For sheet transplantation, two to three retinal sheets were consequently loaded in the bevel of a 21G microneedle with photoreceptor side

facing down, gently aspirated into a Hamilton syringe, and then tangentially injected into the subretinal space (SRS) through the sclera under a surgical microscope (Leica, USA). For suspension transplantation, 2 μl of cells suspensions were transplanted into the SRS following the protocol as described. Successful injection was verified by direct visualization through the dilated pupil of the recipient.

2.5 Immunohistochemistry (IHC) staining

Retina cryosections (10 μm thick) from *OPN1LW-EGFP/NRL*$^{-/-}$, *OPN1LW-EGFP*, *NRL*$^{-/-}$, and *WT* mice, as well as grafted albino *Rd1/NS* mice were collected and stained as previously described (Singh et al., 2016). Briefly, retinal sections were rinsed with PBS (5 min × 2), then permeabilized and blocked using a mixture of 0.1% Triton-X100 and 5% goat serum in PBS for 1 hour at RT. After rinsing in PBS (5 min × 3), retinal sections were incubated with primary antibody overnight at 4°C, rinsed in PBS (5 min × 3) and followed by secondary antibody incubation for one hour at RT, then stained with DAPI and mounted using ProLong Diamond mounting media. Primary and secondary antibodies used were listed in Supplemental Table S2.

2.6 Histology quantification

For temporal colocalization analysis, retina sections from *OPN1LW-EGFP/NRL*$^{-/-}$ mice aged P7 to P35 were double-stained with S-opsin and anti-GFP-FITC. Confocal images were collected from dorsal and ventral retina sections of P7 (n=6 images), P10 (n=9 images), P15 (n=7 images), and P35 (n=4 images) mice. Regions of interest (ROI) were defined as the outer retina using Image J. Co-localized regions on each ROI were identified by automated thresholding using the Costes approach in Imaris. Colocalized volume in each case was designated as “% ROI Colocalized” which equaled the ratio of the colocalized voxel volume to the full ROI volume. Mander’s colocalization coefficient (MCC) was obtained from the voxels that were above the threshold of S-opsin (red channel) and OPN1LW-EGFP (green channel) signal to avoid background interference.

To quantify opsin colocalization, retina flat mounts from *OPN1LW-EGFP/NRL*$^{-/-}$ and *OPN1LW-EGFP* mice (aged P35, n=4 retinae per group) were double-stained with S-opsin and anti-GFP-FITC. Confocal images were collected from the dorsal, mid- (surrounding the optic nerve), and ventral retina (two regions of interest (ROIs) per region, Fig. 1 D2). Cone photoreceptors co-expressing OPN1LW-EGFP and S-opsin ($EGFP^+S^+$) or expressing only OPN1LW-EGFP ($EGFP^+S^-$) or S-opsin ($EGFP^-S^+$) were semi-automatically quantified by the spots colocalization analysis (ComDet v.0.5.5) using Image J. Data were presented as “(opsin subtypes/total cones) %”. Representative 3D images were constituted by Imaris.

For rosette development analysis, mature rosettes were manually quantified on dorsal and ventral tile scan images of retina sections of *OPN1LW-EGFP/NRL*$^{-/-}$ mice (P7, P10, P12, P15: n= 8 sections for each age, P35: n=7 sections) and age-matched *NRL*$^{-/-}$ mice (P7, P10, P12, P35: n=8 sections for each age, P15: n=6 sections) using Image J.

To characterize the cellular composition of rosettes in *OPN1LW-EGFP/NRL*$^{-/-}$ mice, we stained retina sections (n=8–12) of *OPN1LW-EGFP/NRL*$^{-/-}$ mice (P35-P49) with retina specific markers including S-opsin (S-cone), L/M-opsin (M-cone), Rhodopsin (Rho, rod),

GFAP (astrocyte and activated Müller glia), and PKC-α (rod bipolar cell), with age-matched *NRL*$^{-/-}$ retina sections as a control. The percentage of the rosettes expressing certain retinal marker were counted manually using Image J.

For graft quantification, retina cryosections from the sheet-grafted *Rd1/NS* mice (n=16 sections) and suspension-grafted *Rd1/NS* mice (n=20 sections) were selectively stained with anti-GFP-FITC, S-opsin, and L/M-opsin following the aforementioned protocol, then manually quantified using the "cell counter" plugin in Image J.

2.7 Transmission Electron Microscopy (TEM)

Cryostat sections (15 μm thick) from *OPN1LW-EGFP/NRL*$^{-/-}$ eyes were processed for TEM by the Core Microscopy Facility in Johns Hopkins University, as previously reported (Norris and Griffiths, 1983). Retinal sections were fixed with phosphate-buffered glutaraldehyde (2%) at 4°C for 5 minutes prior to processing. Fixed retina sections were rinsed in 0.1 M phosphate buffer with 3% sucrose (Thermo Fisher Scientific, USA) (3 × 2 min), then post-fixed in 2% osmium tetroxide and 1.6% potassium ferrocyanide (Electron Microscopy Sciences (EMS)) on ice in the dark for 45 min. After DD.H_2O rinse (2 × 10 seconds), retina sections were stained with 2% aqueous uranyl acetate (15 min, dark) (Polysciences, Warrington, PA, USA) and dehydrated by a gradient ethanol (30%, 50%, 70%, 90%: 1 × 5 min for each concentration; 100%: 3 × 5 min), then removed into propylene oxide (2 × 5 min) (EMS), embedded in Eponate 12 (EPON) (Ted Pella, Redding, CA) resin, and polymerized at 60°C overnight on inverted BEEM Capsules (Ted Pella; BEEM: Better equipment for Electron Microscopy). The next day, slides were dropped into liquid nitrogen and samples were trimmed to the ROI, cut at 70 nm on a Leica UC7 ultramicrotome (Buffalo Grove, USA), picked up with 2 × 1 mm formvar coated copper slot grids, stained with 2% uranyl acetate in 50% methanol (15 min) and imaged under a Philips CM120 TEM at 80 kV equipped with an AMT XR80 CCD 8megapixel camera.

2.8 Multifocal confocal scanning laser ophthalmoscopy (cSLO) imaging and quantification

Multimodal cSLO imaging was performed on *OPN1LW-EGFP/NRL*$^{-/-}$, *OPN1LW-EGFP*, *NRL*$^{-/-}$, and *WT* mice (aged P36-P49) (*WT* mice: n=9 eyes, other mice: n=10 eyes per strain). Short-wavelength fluorescence (SWF) imaging (488/500nm excitation/emission with automatic real-time (ART) averaging of 52 frames) was used to track OPN1LW-EGFP$^+$ cells. Multicolor reflectance (MR) (>20 ART frames) was used to detect rosettes. Fundus montages of SWF and MR images were created manually to present the distribution of OPN1LW-EGFP$^+$ cells and the rosette, respectively. SD-OCT scanning was recorded through the same area as fundus montage (9 ART frames/scan). Whole retina thickness was quantified on B-scans at a distance of 0.5 μm, 427.2 μm, and 854.4 μm from the optic nerve in both dorsal and ventral retina. The thickness of inner and outer segments (IS/OS), outer nuclear layer and outer limiting membrane (ONL/OLM), and inner retina including outer plexiform layer (OPL), inner nuclear layer (INL), inner plexiform layer (IPL) and retinal ganglion cells (RGC) was measured on the B-scans at the middle distance (427.2 μm) from the optic nerve in the dorsal retina. Each retina section on selected OCT images was evenly divided into three parts by two vertical lines (Line A across the 1/3 of the retina length, Line

B across the 2/3 of the retina length). Retinal thicknesses were measured along with the Line A (Thickness 1) and Line B (Thickness 2) using image J. Mean value of “Thickness 1” and “Thickness 2” was used for statistical analysis.

For transplantation study, multimodal cSLO imaging was performed on grafted *Rd1/NS* mice at 1 month and 3 months post-transplantation, as previously reported (Liu et al., 2020). SWF imaging was used to track the retinal graft. SD-OCT scanning through the grafted area was recorded for a detailed investigation of graft and recipient retinal status. The SWF^+ graft area and the SWF signal intensity was quantified using Image J. Graft thickness was measured on the SD-OCT images as mentioned above. The change ratios of the SWF^+ graft area, SWF signal intensity, and SD-OCT thickness were expressed as “(three-month value/one-month value)% ”.

2.9 Electroretinography (ERG)

Full-field ERGs were recorded on *OPN1LW-EGFP/NRL*$^{-/-}$, *OPN1LW-EGFP*, *NRL*$^{-/-}$, and *WT* mice (n=10 eyes/strain) using the Espion system (Diagnosys LLC, Lowel, USA). Mice (P36~P45) were dark-adapted overnight, anesthetized under dim red light. Pupils were dilated with 1% (*WT*/vol) tropicamide. A drop of 2% methylcellulose was put on the cornea to keep it hydrated. Scotopic ERG was recorded under white-flash stimuli with six intensity series (− 4.4 to +0.6 log cd.s/m^2). For dim stimuli (− 4.4 to − 2.4 log cd.s/m^2), three responses were averaged with an interstimulus interval (ISI) of 5 seconds. For high intensities (− 1.4 to +0.6 log cd.s/m^2), three responses were averaged with an ISI of 10 or 15 seconds. Following scotopic ERG, 10 minutes light adaptation was performed on each case under white light (30 cd/m^2). Photopic ERG was then recorded under white-flash stimuli over five intensities ranging from −1.4 to +0.6 log cd.s/m^2. Three responses were averaged for each intensity with an ISI of 1 second (−1.4 to +0.1 log cd.s/m^2) or 1.5 seconds (0.6 log cd.s/m^2). Consequently, 465 nm and 525 nm chromatic stimuli were imposed on a 30 cd/m^2 white background using the same intensity series and ISI as photopic ERG, and responses were averaged for three records.

2.10 Statistics

Quantitative data were analyzed using either a two-way ANOVA or one-way ANOVA. Sidak’s test or Tukey’s test was adopted for multiple comparison (two-tailed). Independent T-test or Mann-Whitney U test was adopted for two variances comparison. SPSS (version 25, IL, USA) was used for statistical analysis. Graphpad Prism (version 8, CA, USA) was used for graph generation. $p < 0.05$ was taken to be significant.

3. Results

3.1 $EGFP^+$ and L/M $opsin^+$ cells distribution

We performed *in vivo* SWF imaging on *OPN1LW-EGFP/NRL*$^{-/-}$ and three control lines (*OPN1LW-EGFP*, *NRL*$^{-/-}$, and *WT*). There were more $EGFP^+$ photoreceptors in *OPN1LW-EGFP/NRL*$^{-/-}$ mice than *OPN1LW-EGFP* mice (Fig. 1). The EGFP photoreceptors were distributed along a dorsal-ventral density gradient, with a higher density in the dorsal than in the ventral retina. We did not detect a strong *in vivo* SWF signal in *NRL*$^{-/-}$and *WT*

mice. However, we found relatively dim *in vivo* auto-fluorescent dots in the ventral *NRL*$^{-/-}$ retina (Fig. 1A). These dots correlated anatomically with outer retinal rosettes on SD-OCT imaging (Supplemental Fig. S1).

In flat mounts of *OPN1LW-EGFP/NRL*$^{-/-}$ mice, EGFP expression was enriched in the dorsal and the ventral retina, compared to *OPN1LW-EGFP* controls (dorsal: 39.01 ± 7.60 vs 23.38 ± 3.89, $p < 0.0001$; ventral: 12.14 ± 7.02 vs 4.51 ± 2.11, $p = 0.03$; in *OPN1LW-EGFP/NRL*$^{-/-}$ and *OPN1LW-EGFP* respectively; n = 9 eyes/strain) (Fig. 1B–C).

We sought to evaluate the extent to whether EGFP density distribution paralleled L/M-opsin expression in *OPN1LW-EGFP/NRL*$^{-/-}$ mice. Ventral retinal L/M-opsin density was slightly higher in *OPN1LW-EGFP/NRL*$^{-/-}$ than in *OPN1LW-EGFP* and *NRL*$^{-/-}$ (Fig. 1B–C). Dorsal L/M-opsin density was slightly higher in *OPN1LW-EGFP/NRL*$^{-/-}$ than in *NRL*$^{-/-}$ whereas less than in *OPN1LW-EGFP* and *WT*, with WT showed significance (n= 5 eyes/strain, $p = 0.04$). Qualitatively, numerous *OPN1LW-EGFP/NRL*$^{-/-}$ cells expressed L/M-opsin but not EGFP (Fig. 1B).

3.2 S-opsin density distribution

The mean density of S-opsin in the dorsal retina of *OPN1LW-EGFP/NRL*$^{-/-}$ mice was higher than in *OPN1LW-EGFP* and *WT* mice (17.20 ± 4.37 vs. 1.54 ± 0.70 and 1.64 ± 2.01 respectively; n = 4–5 eyes per group, $p < 0.0001$) (Fig. 1C). A heat map summarized the density distribution of opsin and EGFP a similar dorsal-ventral gradient of S-opsin distribution in *OPN1LW-EGFP/NRL*$^{-/-}$ and *NRL*$^{-/-}$ mice (Fig. 1C).

We observed numerous EGFP cells that co-expressed S-opsin on retinal flat-mount staining (Fig. 1B). To investigate the temporal characteristic of S-opsin and OPN1LW-EGFP co-expression, sections from P7 to P35 *OPN1LW-EGFP/NRL*$^{-/-}$ retinas were double-stained with S-opsin and anti-GFP-FITC. OPN1LW-EGFP expression gradually increased from P7 to P35 and S-opsin expression appeared relatively stable during that interval (Fig. 1 D1). OPN1LW-EGFP and S-opsin colocalization in the outer retina increased from P7 to P15 and then declined until P35 (Fig.1 D1, yellow line). Individual fraction changes of OPN1LW-EGFP and S-opsin signal in colocalized compartments were analyzed via MCC (denoted as MCC_G and MCC_R, respectively) (Fig.1 D1, green and red lines). The MCC_G significantly declined from P7 to P15 (0.30 ± 0.10 vs. 0.11 ± 0.08, n = 6–7 per time point, $p = 0.01$) and then remained stable until P35 (0.13 ± 0.04). MCC_R increased from P7 to P15 (2.45-fold higher than MCC_G, n= 7 images, $p = 0.03$) and then declined until P35.

We sought to evaluate whether the *NRL*$^{-/-}$ background shifted the ratio of cones that co-expressed S-opsin and OPN1LW-EGFP in *OPN1LW-EGFP/NRL*$^{-/-}$ mice compared with *NRL*$^{+/+}$ mice. Retina flat mounts from P35 *OPN1LW-EGFP/NRL*$^{-/-}$ and *OPN1LW-EGFP* mice were double-stained with S-opsin and anti-GFP-FITC for quantification. The percentage of cones co-expressing OPN1LW-EGFP and S-opsin ($EGFP^+S^+$) in *OPN1LW-EGFP/NRL* $^{-/-}$ was significantly higher than in *OPN1LW-EGFP* retinae (dorsal: 20.17 ± 6.37% vs. 1.57 ± 0.65%, $p < 0.0001$; mid: 14.47 ± 6.79% vs. 4.48 ± 4.74%, $p = 0.0002$; ventral: 10.97 ± 2.29% vs. 5.11 ± 3.21%, $p = 0.04$; n = 4 eyes/group). While the OPN1LW-EGFP-only cones ($EGFP^+S^-$) and the S-opsin-only cones ($EGFP^-S^+$) in

OPN1LW-EGFP/NRL$^{-/-}$ followed a similar dorsal-ventral gradient as in the *OPN1LW* retina, EGFP^{+}S^{-} cones accounted for a much smaller portion of cone photoreceptors in *OPN1LW-EGFP/NRL*$^{-/-}$ than in *OPN1LW*. In contrast, the EGFP^{-}S^{+}-cones were significantly more frequent in *OPN1LW-EGFP/NRL*$^{-/-}$ than in *OPN1LW* retina. (Fig. 1 D2–D4).

3.3 Time course of rosette development and involution

The rosettes of *NRL*$^{-/-}$ mice emitted a dim SWF signal (Fig. 1A). We could not detect this dim signal in *OPN1LW-EGFP/NRL*$^{-/-}$ mice against the bright EGFP-related SWF signal. Multimodal imaging data showed that the numerous green circles in the ventral retina of *OPN1LW-EGFP/NRL*$^{-/-}$ and *NRL*$^{-/-}$ mice detected on MR imaging correlated with outer retinal rosettes detected on SD-OCT imaging (Fig. 2A).

At P7 in *OPN1LW-EGFP/NRL*$^{-/-}$ and *NRL*$^{-/-}$ mice, S-opsin expression was localized at the outer boundary of the outer nuclear layer, with no rosette formation. Qualitatively, the morphology of the rosettes evolved from P10 to P35, from nascent to mature rosettes(Stuck et al., 2012). Mature rosettes in *OPN1LW-EGFP/NRL*$^{-/-}$ retina were rarely observed at P7, but increased from P10 to P15 and then reduced decreased until P35. The retina structure was marred by rosettes between P12 and P15. Improved retinal lamination was observed at P35. This time course was similar in *OPN1LW-EGFP/NRL*$^{-/-}$ and *NRL*$^{-/-}$ mice. Mature rosettes were more numerous in *OPN1LW-EGFP/NRL*$^{-/-}$ than *NRL*$^{-/-}$ mice at P15 (41.5 ± 9.8 vs 30.3 ± 13.3, $p = 0.02$, Fig. 2B).

3.4 Retinal thinning in *OPN1LW-EGFP/NRL*$^{-/-}$ mice

The *OPN1LW-EGFP/NRL*$^{-/-}$ retina at 5 – 6w was thinner than in age-matched *OPN1LW-EGFP*, *NRL*$^{-/-}$, and *WT* controls at the distances of 427.2 μm and 854.4 μm, in both dorsal and ventral retina. Detailed analysis at the distance of 427.2 μm showed that the *OPN1LW-EGFP/NRL*$^{-/-}$ retinal thinning involved the outer retina. The mean IS/OS length of the *OPN1LW-EGFP/NRL*$^{-/-}$ retina was less than that of *OPN1LW-EGFP* and *WT* retinas, but similar to *NRL*$^{-/-}$ retinas. The ONL and OLM in *OPN1LW-EGFP/NRL*$^{-/-}$ were thinner than controls. The inner retina thickness was similar across the mouse lines studied (Fig. 2C).

3.5 Cellular composition of rosettes

OPN1LW-EGFP^{+} photoreceptors were detected in almost all of the rosettes (> 99%) (Fig. 3A). Three-dimensional reconstruction confirmed that that S-opsin^{+} and L/M-opsin^{+} structures were concentrated in rosette centers (Fig. 3B). *OPN1LW-EGFP/NRL*$^{-/-}$ retinas contained more S-opsin^{+} rosettes than *NRL*$^{-/-}$ retinas (74.57 ± 13.48 % vs 46.61 ± 20.04 %, n =11 – 12 each), $p < 0.0001$). The percentage of L/M-opsin^{+} rosettes in the *OPN1LW-EGFP/NRL*$^{-/-}$ retinas were not significantly different than in *NRL*$^{-/-}$ retinas. Rod photoreceptors (Rho^{+}) were observed in ~ 2.63% of rosettes in *OPN1LW-EGFP/NRL*$^{-/-}$ mice and ~ 2.78% in *NRL*$^{-/-}$ mice, without a statistically significant difference. Glial cells, indicated by GFAP^{+} staining, were observed in ~ 43% of rosettes in *OPN1LW-EGFP/NRL*$^{-/-}$ mice and ~52% in *NRL*$^{-/-}$ mice, without a statistically significant difference (Fig. 3C). TEM revealed the microstructure of *OPN1LW-EGFP/NRL*$^{-/-}$ rosettes, including

the presence of OLM-like structures inside the rosettes. There were individually visible inner segments and connecting cilia. Outer segments contained disorganized disks (Fig. 3D).

3.6 Functional responses to different ERG stimulus wavelengths

Given the enrichment of cone photoreceptors in *OPN1LW-EGFP/NRL*$^{-/-}$ retina, we sought to correlate the anatomical features with retinal function.

Dark-adapted (scotopic) intensity response series (−4.4 to +0.6 log cd.s/m^2) revealed the absence of detectable a-waves in *OPN1LW-EGFP/NRL*$^{-/-}$ and *NRL*$^{-/-}$ mice at all tested intensities (Fig. 4A–B). Scotopic b-waves were non-detectable in *OPN1LW-EGFP/NRL*$^{-/-}$ and *NRL*$^{-/-}$ mice across intensities from −4.4 to −1.4 cd.s/m^2 but were just detectable at −0.4 and +0.6 log cd.s/m^2 stimulus intensity. The mean light-adapted (photopic) b-wave response amplitude of *OPN1LW-EGFP/NRL*$^{-/-}$ mice was significantly lower than *OPN1LW-EGFP* mice at 0.1 log cd.s/m^2 stimulus intensity, and lower than all control mice at 0.6 log cd.s/m^2 stimulus intensity.

We sought to identify if differential light-adapted responses would be obtained with stimuli of differing wavelength, i.e., 465 nm and 525 nm. The mean b-wave response amplitude with the 465 nm stimulus was greater in *OPN1LW-EGFP/NRL*$^{-/-}$ mice compared to *OPN1LW-EGFP* and *WT* mice at high intensities, with statistical significance observed at 0.6 cd.s/m^2 stimulus intensity. The mean b-wave response amplitude with the 525 nm stimulus was lower in *OPN1LW-EGFP/NRL*$^{-/-}$ mice compared to *OPN1LW-EGFP* and *WT* mice at 0.1 and 0.6 cd.s/m^2 stimulus intensities. In *OPN1LW-EGFP/NRL*$^{-/-}$ mice, the mean photopic b-wave response amplitude with the 465 nm stimulus was higher than with the 525 nm stimulus, with statistical significance observed at stimulus intensities of 0.1 and 0.6 cd.s/m^2 (Fig. 4B).

3.7 Transplantation of *OPN1LW-EGFP/NRL*$^{-/-}$ retinal sheets and cell suspensions

Cone-rich retinal sheets and suspensions from P6 *OPN1LW-EGFP/NRL*$^{-/-}$ mice were injected subretinally into a murine retinal degeneration mice model with immune deficiency (*Rd1/NS* mice). EGFP reporter expression enabled the longitudinal tracking of grafted cones by multi-modal cSLO imaging. One-month post-transplantation, the presence and topographical distribution of the grafted retinal sheets and suspensions were indicated by the bright SWF signal. SD-OCT scanning showed that the grafted retinal sheet and suspension was located in the subretinal space of the recipient retina and was in a planar configuration. Three months post-transplantation, the grafted sheets showed a brighter SWF signal than at month-one graft (Fig. 5A). No obvious change was found in the grafted retinal sheets on SD-OCT imaging up to three months after transplantation.

We quantified the change ratio of graft area, EGFP intensity (per SWF imaging), and thickness (per SD-OCT imaging) from one month to three months. The suspension graft had greater reductions ratio of area, EGFP intensity, and thickness than the sheet grafts from one to three months post-transplantation (Fig. 5A–B). Noting that the O*PN1LW-EGFP/NRL*$^{-/-}$ retina lacked residual rod photoreceptors, we estimated the quantity non-photoreceptors in the grafts based on the non-cone fraction. We found the donor-derived non-photoreceptor retinal cells were significantly less in sheet grafts than in the suspension grafts at three

months (52.5 ±17.0% vs. 85.0 ± 8.8%, $p<0.0001$). We found the grafted retinal cells from *OPN1LW-EGFP* heterozygotes were not detectable by SWF imaging (data not shown). EGFP+ cells were not detected in the recipient inner retinal layers.

Three months after transplantation, the sheet grafts contained OPN1LW-EGFP$^+$ cone photoreceptors with occasional elongated neurites (Fig. 5C). Most of the suspension grafts lacked a detectable SWF signal three months post-transplantation. IHC staining using anti-GFP antibody highlighted OPN1LW-EGFP$^+$ cone photoreceptors in sheet and suspension grafts. Both types of grafts contained more OPN1LW-EGFP$^+$ photoreceptors than the P6 donor retina (Fig. 5D). However, the mean percentage of OPN1LW-EGFP$^+$ photoreceptors in suspension grafts was less than in sheet grafts (37.61 ± 11.38 vs. 10.70 ± 5.53%, $p<0.0001$) (Fig. 5C, D). The difference in L/M-opsin$^+$ photoreceptor content between sheet and suspension grafts was nonsignificant (1.38% vs. 0.11%) (Fig. 5C, D). We found greater abundance of S-opsin$^+$ photoreceptors in the sheet graft than in P6 donor controls or in suspension grafts (Fig. 5D). There were more S-opsin$^+$ than L/M-opsin$^+$ photoreceptors in both sheet and suspension grafts (Fig. 5C, D).

4. Discussion

The data show that the retinal phenotypes of *OPN1LW-EGFP/NRL*$^{-/-}$ and *NRL*$^{-/-}$ mice are similar but not identical. We considered the relative abundance, distribution, and functionality of cone opsin-expressing cells as the most important features to study, in the context of potentially using donor *OPN1LW-EGFP/NRL*$^{-/-}$ photoreceptor cells in allogeneic transplantation studies. Anatomically, the cone photoreceptor enrichment in *NRL*$^{-/-}$ retinas appeared to be unaffected by the introduction of the *OPN1LW-EGFP* reporter. The relative proportion of S opsin- and L/M opsin-expressing cells was similarly unaffected, as was the dorsal-ventral distribution pattern of these cells. The occurrence of outer retinal rosettes was also similar. However, we found potentially important differences in terms of cone photoreceptor function. We validated the use of this donor strain for transplantation studies, particularly for studies involving *in vivo* SWF imaging as an outcome measure.

In designing our experiments, we considered the lack of an available *OPN1SW-EGFP* mouse line that would directly label S-opsin expressing cones. However, it is recognized that M- and S-opsins are co-expressed in several mammals (Applebury et al., 2000; Lukats et al., 2002; Parry and Bowmaker, 2002; Peichl, 2005; Rohlich et al., 1994; Williams and Jacobs, 2007), including *NRL*$^{-/-}$ mice (Nikonov et al., 2005). The mouse model herein contains increased S-opsin expressing cones with *OPN1LW-EGFP* reporter (~15%) compared to *OPN1LW-EGFP* mice (~4%), serving as a histological sentinel for graft localization and facilitating S-opsin immunolabeling, where needed, in neighboring GFP– cones. The *in vivo* imaging and histological observations are in keeping with co-expression of M- and S-opsin in a portion of cones in the *OPN1LW-EGFP/NRL*$^{-/-}$ model. In addition, the *NRL*$^{-/-}$ background increased the S-opsin-only cones across the whole retina compared to the wild-type *NRL*$^{+/+}$ retina (Nadal-Nicolas et al., 2020) and this may account for GFP detection in S-cones herein. Developing an endogenous S-opsin reporter strategy for direct labeling of S-opsin$^+$ cones in this line may offer rational approach for further characterization of the *OPN1LW-EGFP/NRL*$^{-/-}$ retina.

Published data on the characteristics of *Nrl*$^{-/-}$ photoreceptors (Daniele et al., 2005) highlight limitations of using them to model wildtype cone transplantation. Electrophysiologically, *Nrl*$^{-/-}$ photoreceptors show a spectral sensitivity profile that incorporates the wavelength specificity of both mouse S- and M-opsin. This may pose a challenge in assessing opsin function separately or in discrete cells. Furthermore, the outer segments of *Nrl*$^{-/-}$ photoreceptors are shorter than wild-type cones, thus likely influencing histological interpretation and maximal electrical response amplitudes. While molecular, structural, and functional similarities exist between *Nrl*$^{-/-}$ photoreceptors and wild-type cones, these important caveats must be considered when studying transplantation outcomes in mice.

Photoreceptor rosettes are known to form temporarily in *NRL*$^{-/-}$ mice (Stuck et al., 2012), and leave a legacy of stable retinal thinning after their disappearance. Our data show that the overall time course of increase and subsequent decrease of rosettes in the *NRL*$^{-/-}$ mouse was not affected by the addition of *OPN1LW-EGFP* reporter. However, the addition of this reporter increased the maximum number of rosettes formed, although the mechanism of this change is unclear. We found that accelerated ONL degeneration, as early as 35 days of age, occurred in *OPN1LW-EGFP/NRL*$^{-/-}$ retinas (versus at two to four months in *NRL*$^{-/-}$ retina (Mears et al., 2001)). Whether this difference is related to direct insertional mutagenesis of *OPN1LW-EGFP* in *NRL*$^{-/-}$ retina (Lipinski et al., 2011) or an indirect consequence of increased rosette formation, or both, is a question that requires further study.

Several mechanisms of rosette formation have been proposed (Chuang et al., 2010; Mehalow et al., 2003; Morarji et al., 2016), including aberrant photoreceptors maturation of OLM disruption(Stuck et al., 2012), and cis-retinoid exposure (Feathers et al., 2008; Kunchithapautham et al., 2009). Notably, we found segments of OLM, IS, and/or OS inside the rosettes of *OPN1LW-EGFP/NRL*$^{-/-}$ retina. These findings show some similarities with the characteristics of outer retinal tubulation (ORT) in advanced human AMD (Curcio et al., 1996; Medeiros and Curcio, 2001; Schaal et al., 2015). Cone enrichment and Müller cell interactions were considered to underlie the preferential formation of ORT in the macula region in the human retina (Anderson et al., 1986; Curcio et al., 1996; Schaal et al., 2015). In our study, we found GFAP^{+} Müller cells interleaved long processes between cone photoreceptors in rosettes, implying a potential role of Müller cells in rosette formation in *OPNL1L-EGFP/NRL*$^{-/-}$ retina.

Rosette formation in *OPN1LW-EGFP/NRL*$^{-/-}$ retina may pose a barrier to effective photoreceptor integration into recipient mice and may affect donor cell survival post-transplantation. To ameliorate these potential problems, harvesting dorsal retinal tissue for transplantation may be advantageous, given the ventral predominance of rosettes. We found that grafted cone photoreceptors survived and formed rare rosettes (less than 1%) in sheet grafts at one month post-transplantation. Collecting the donor sheets from around P6 might alleviate rosette formation and facilitate donor cell survival in sheet grafts. While purification of EGFP^{+} cones from a rosette-limit stage is possible as early as P6 in *OPN1LW-EGFP/NRL*$^{-/-}$ mice, the peak of OPN1LW-EGFP and S-opsin co-expression is seen at the relatively rosette-rich stage of P15. An appropriate donor mouse age should be considered depending on goal of particular experiments. Using a cone-enriched mouse that lacks rosettes due to genetic manipulation (*R91W;NRL*$^{-/-}$) (Samardzija et al., 2014)

is another alternative, depending on the experimental tolerance for the consequences of the *R91W* mutation on donor cone function. Further study of rosette pathophysiology may facilitate the development of strategies to reduce or eliminate rosettes after transplantation, thus improving the laminar organization of the reconstructed outer retina. We found, unexpectedly, that MR imaging was a useful tool to detect retinal rosettes in mice. As an assay of the quantity and regional distribution in living animals, MR imaging may enable further quantitative research in rosette pathophysiology in rodents.

We used chromatic full-field stimuli to provide differential stimulation of L/M- and S-cones. Mouse L/M- and S-cones are maximally sensitive near 508 nm and 360 nm stimuli, respectively. We found that the light-adapted retinal response to 525 nm, but not 465 nm, stimulation was lower in *OPN1LW-EGFP/NRL*$^{-/-}$ than in *NRL*$^{-/-}$ mice. This finding indicated a significant functional consequence of *OPN1LW-EGFP* reporter insertion in the *NRL*$^{-/-}$ retina, wherein L/M-cone function was reduced to a greater extent than S-cone function. Anatomically, greater photoreceptor layer thinning in the *OPN1LW-EGFP/NRL*$^{-/-}$ than *NRL*$^{-/-}$ mice may account for the reduced function in the former strain. Another explanation could be that EGFP expression impairs phototransduction in L/M-cones. With the 465 nm stimulus, that we presumed would more selectively (but not exclusively) stimulate S- rather than L/M-cones, we found responses in the *OPN1LW-EGFP/NRL*$^{-/-}$ that concur with known data on S-cone enrichment in the *NRL*$^{-/-}$ line. More in depth ERG studies were beyond the scope of the current work, but the functional phenotype of L/M- and S-cones in this line may be studied with greater precision by using selective background suppression (Arden et al., 1999) or ultraviolet stimulation (Hunt and Peichl, 2014). Moreover, comprehensive functional evaluations, such as whether the functional cone photoreceptors of *OPN1LW-EGFP/NRL*$^{-/-}$ mice could reconstitute the visual function of recipient mice, and whether the functional shifts of cone subtypes in *OPN1LW-EGFP/NRL*$^{-/-}$ mice would contribute to functional recovery differences after transplantation, should be explored in future studies.

In general, less is known about cone photoreceptor transplantation than that of rods. The rarity of cone photoreceptors in the mouse (3% of photoreceptor cells) presents a challenge for harvesting sufficient cones, and purifying them, for transplantation experiments (Kruczek et al., 2017; Smiley et al., 2016a and 2016b; Waldron et al., 2018). Pooling dissociated and sorted cells from multiple recipients is one solution. However, the dissociation and sorting process is considered harmful to delicate cone photoreceptors (Nikonov et al., 2006). We found that the *OPN1LW-EGFP/NRL*$^{-/-}$ mice provided an abundant source of donor cone cells and thus eliminated the need for purification. In addition, robust tracking of grafted EGFP-labeled cones over time required a detectable SWF signal; in this respect we found it critical to use EGFP homozygotes.

5. Conclusion

OPN1LW-EGFP/NRL$^{-/-}$ retinae were enriched with traceable S-opsin^{+} photoreceptor cells. Sustained expression of EGFP facilitated the long-term tracking of donor cells for at least three months following transplantation, facilitating long-term observation of cone photoreceptor maturation and function. Homozygosity for *OPN1LW-EGFP* altered the

structural and functional characteristics of *NRL*$^{-/-}$ mice, causing retinal thinning and reducing cone photoreceptor-driven retinal responses compared to *NRL*$^{-/-}$ mice without the reporter construct. Transplantation studies using this model should consider reduced donor function, structural differences between wild-type and *NRL*$^{-/-}$ photoreceptors, and the time course of rosette formation and involution, when evaluating anatomical and functional outcomes. Photoreceptor sheet transplantation may promote greater macroscopic graft integrity and S-opsin^{+} photoreceptor survival than cell suspension transplantation. With further study, this novel cone-rich reporter mouse line may be useful for studying the influence of graft structure on cone subtype survival. Greater understanding of the relationship between those parameters may inform the development of clinically-relevant cone photoreceptor regeneration strategies.

Supplementary Material

Refer to Web version on PubMed Central for supplementary material.

Acknowledgments

We thank Dr. Elia Duh and Dr. Hongkwan Cho for their kind help with ERG training. We thank Barbara Smith for her kind help with TEM.

Funding:

This work was supported by the Foundation Fighting Blindness (Career Development Award to MSS), The Shulsky Foundation, the Juliette RP Vision Foundation, Research to Prevent Blindness (unrestricted grant to the Wilmer Eye Institute), and the National Eye Institute Core Grant EY001765.

Abbreviations

EGFP	enhanced green fluorescent protein
cSLO	confocal scanning laser ophthalmoscopy
AMD	age-related macular degeneration
RP	retinitis pigmentosa
NRL	neural retina leucine
GFP	green fluorescent protein
MACS	magnetic-activated cell sorting
WT	wild-type
rd1	C3H/HeJ-Pde6br;d1
NS	NOD.CB17-Prkdcscid/J
Rd1/NS	C3H/HeJ-Pde6brd;NOD.CB17-Prkdcscid/J
PFA	paraformaldehyde
PBS	phosphate-buffered saline

RT	room temperature
IHC	immunohistochemistry
ROI	Regions of interest
MCC	Mander's colocalization coefficient
TEM	transmission Electron Microscopy
SWF	short-wavelength fluorescence
MR	multicolor reflectance
SD-OCT	spectral-domain optical coherence tomography
ART	automatic real-time
IR	infrared
IS	inner segments
OS	outer segments
CC	connecting cilium
ONL	outer nuclear layer
OLM	outer limited membrane
OPL	outer plexiform layer
INL	inner nuclear layer
IPL	inner plexiform layer
RGC	retinal ganglion cell
ERG	electroretinography
ISI	interstimulus interval

References

Akimoto M, Cheng H, Zhu D, Brzezinski JA, Khanna R, Filippova E, Oh EC, Jing Y, Linares JL, Brooks M, Zareparsi S, Mears AJ, Hero A, Glaser T, Swaroop A, 2006. Targeting of GFP to newborn rods by Nrl promoter and temporal expression profiling of flow-sorted photoreceptors. Proc Natl Acad Sci U S A103, 3890–3895. [PubMed: 16505381]

Anderson DH, Guerin CJ, Erickson PA, Stern WH, Fisher SK, 1986. Morphological recovery in the reattached retina. Invest Ophthalmol Vis Sci27, 168–183. [PubMed: 3943943]

Applebury ML, Antoch MP, Baxter LC, Chun LL, Falk JD, Farhangfar F, Kage K, Krzystolik MG, Lyass LA, Robbins JT, 2000. The murine cone photoreceptor: a single cone type expresses both S and M opsins with retinal spatial patterning. Neuron27, 513–523. [PubMed: 11055434]

Arden G, Wolf J, Berninger T, Hogg CR, Tzekov R, Holder GE, 1999. S-cone ERGs elicited by a simple technique in normals and in tritanopes. Vision Res39, 641–650. [PubMed: 10341991]

Brooks MJ, Chen HY, Kelley RA, Mondal AK, Nagashima K, De Val N, Li T, Chaitankar V, Swaroop A, 2019. Improved Retinal Organoid Differentiation by Modulating Signaling Pathways Revealed by Comparative Transcriptome Analyses with Development In Vivo. Stem Cell Reports13, 891–905. [PubMed: 31631019]

Chang B, Dacey MS, Hawes NL, Hitchcock PF, Milam AH, Atmaca-Sonmez P, Nusinowitz S, Heckenlively JR, 2006. Cone photoreceptor function loss-3, a novel mouse model of achromatopsia due to a mutation in Gnat2. Invest Ophthalmol Vis Sci47, 5017–5021. [PubMed: 17065522]

Chen Y, Ratnam K, Sundquist SM, Lujan B, Ayyagari R, Gudiseva VH, Roorda A, Duncan JL, 2011. Cone photoreceptor abnormalities correlate with vision loss in patients with Stargardt disease. Invest Ophthalmol Vis Sci52, 3281–3292. [PubMed: 21296825]

Chichagova V, Dorgau B, Felemban M, Georgiou M, Armstrong L, Lako M, 2019. Differentiation of Retinal Organoids from Human Pluripotent Stem Cells. Curr Protoc Stem Cell Biol50, e95. [PubMed: 31479596]

Chuang JZ, Chou SY, Sung CH, 2010. Chloride intracellular channel 4 is critical for the epithelial morphogenesis of RPE cells and retinal attachment. Mol Biol Cell21, 3017–3028. [PubMed: 20610659]

Curcio CA, Medeiros NE, Millican CL, 1996. Photoreceptor loss in age-related macular degeneration. Invest Ophthalmol Vis Sci37, 1236–1249. [PubMed: 8641827]

Daniele LL, Lillo C, Lyubarsky AL, Nikonov SS, Philp N, Mears AJ, Swaroop A, Williams DS, Pugh EN Jr., 2005. Cone-like morphological, molecular, and electrophysiological features of the photoreceptors of the Nrl knockout mouse. Invest Ophthalmol Vis Sci46, 2156–2167. [PubMed: 15914637]

Eldred KC, Hadyniak SE, Hussey KA, Brenerman B, Zhang PW, Chamling X, Sluch VM, Welsbie DS, Hattar S, Taylor J, Wahlin K, Zack DJ, Johnston RJ Jr., 2018. Thyroid hormone signaling specifies cone subtypes in human retinal organoids. Science362.

Feathers KL, Lyubarsky AL, Khan NW, Teofilo K, Swaroop A, Williams DS, Pugh EN Jr., Thompson DA, 2008. Nrl-knockout mice deficient in Rpe65 fail to synthesize 11-cis retinal and cone outer segments. Invest Ophthalmol Vis Sci49, 1126–1135. [PubMed: 18326740]

Fei Y, Hughes TE, 2001. Transgenic expression of the jellyfish green fluorescent protein in the cone photoreceptors of the mouse. Vis Neurosci18, 615–623. [PubMed: 11829307]

Homma K, Okamoto S, Mandai M, Gotoh N, Rajasimha HK, Chang YS, Chen S, Li W, Cogliati T, Swaroop A, Takahashi M, 2013. Developing rods transplanted into the degenerating retina of Crx-knockout mice exhibit neural activity similar to native photoreceptors. Stem Cells31, 1149–1159. [PubMed: 23495178]

Hunt DM, Peichl L, 2014. S cones: Evolution, retinal distribution, development, and spectral sensitivity. Vis Neurosci31, 115–138. [PubMed: 23895771]

Hurlbert AC, Bramwell DI, Heywood C, Cowey A, 1998. Discrimination of cone contrast changes as evidence for colour constancy in cerebral achromatopsia. Exp Brain Res123, 136–144. [PubMed: 9835402]

Kim S, Lowe A, Dharmat R, Lee S, Owen LA, Wang J, Shakoor A, Li Y, Morgan DJ, Hejazi AA, Cvekl A, DeAngelis MM, Zhou ZJ, Chen R, Liu W, 2019. Generation, transcriptome profiling, and functional validation of cone-rich human retinal organoids. Proc Natl Acad Sci U S A116, 10824–10833. [PubMed: 31072937]

Kruczek K, Gonzalez-Cordero A, Goh D, Naeem A, Jonikas M, Blackford SJI, Kloc M, Duran Y, Georgiadis A, Sampson RD, Maswood RN, Smith AJ, Decembrini S, Arsenijevic Y, Sowden JC, Pearson RA, West EL, Ali RR, 2017. Differentiation and Transplantation of Embryonic Stem Cell-Derived Cone Photoreceptors into a Mouse Model of End-Stage Retinal Degeneration. Stem Cell Reports8, 1659–1674. [PubMed: 28552606]

Kunchithapautham K, Coughlin B, Crouch RK, Rohrer B, 2009. Cone outer segment morphology and cone function in the Rpe65−/− Nrl−/− mouse retina are amenable to retinoid replacement. Invest Ophthalmol Vis Sci50, 4858–4864. [PubMed: 19407011]

Li L, Rao KN, Zheng-Le Y, Hurd TW, Lillo C, Khanna H, 2015. Loss of retinitis pigmentosa 2 (RP2) protein affects cone photoreceptor sensory cilium elongation in mice. Cytoskeleton (Hoboken)72, 447–454. [PubMed: 26383048]

Lipinski DM, Yusuf M, Barnard AR, Damant C, Charbel Issa P, Singh MS, Lee E, Davies WL, Volpi EV, MacLaren RE, 2011. Characterization of a dominant cone degeneration in a green fluorescent protein-reporter mouse with disruption of Loci associated with human dominant retinal dystrophy. Invest Ophthalmol Vis Sci52, 6617–6623. [PubMed: 21705682]

Liu YV, Sodhi SK, Xue G, Teng D, Agakishiev D, McNally MM, Harris-Bookman S, McBride C, Konar GJ, Singh MS, 2020. Quantifiable In Vivo Imaging Biomarkers of Retinal Regeneration by Photoreceptor Cell Transplantation. Translational Vision Science &Technology9, 5.

Lukats A, Dkhissi-Benyahya O, Szepessy Z, Rohlich P, Vigh B, Bennett NC, Cooper HM, Szel A, 2002. Visual pigment coexpression in all cones of two rodents, the Siberian hamster, and the pouched mouse. Invest Ophthalmol Vis Sci43, 2468–2473. [PubMed: 12091452]

MacLaren RE, Pearson RA, MacNeil A, Douglas RH, Salt TE, Akimoto M, Swaroop A, Sowden JC, Ali RR, 2006. Retinal repair by transplantation of photoreceptor precursors. Nature444, 203–207. [PubMed: 17093405]

Makiyama Y, Ooto S, Hangai M, Takayama K, Uji A, Oishi A, Ogino K, Nakagawa S, Yoshimura N, 2013. Macular cone abnormalities in retinitis pigmentosa with preserved central vision using adaptive optics scanning laser ophthalmoscopy. PLoS One8, e79447. [PubMed: 24260224]

Mandai M, Fujii M, Hashiguchi T, Sunagawa GA, Ito SI, Sun J, Kaneko J, Sho J, Yamada C, Takahashi M, 2017. iPSC-Derived Retina Transplants Improve Vision in rd1 End-Stage Retinal-Degeneration Mice. Stem Cell Reports8, 1112–1113. [PubMed: 28402835]

Mears AJ, Kondo M, Swain PK, Takada Y, Bush RA, Saunders TL, Sieving PA, Swaroop A, 2001. Nrl is required for rod photoreceptor development. Nat Genet29, 447–452. [PubMed: 11694879]

Medeiros NE, Curcio CA, 2001. Preservation of ganglion cell layer neurons in age-related macular degeneration. Invest Ophthalmol Vis Sci42, 795–803. [PubMed: 11222543]

Mehalow AK, Kameya S, Smith RS, Hawes NL, Denegre JM, Young JA, Bechtold L, Haider NB, Tepass U, Heckenlively JR, Chang B, Naggert JK, Nishina PM, 2003. CRB1 is essential for external limiting membrane integrity and photoreceptor morphogenesis in the mammalian retina. Hum Mol Genet12, 2179–2189. [PubMed: 12915475]

Morarji J, Lenassi E, Black GC, Ashworth JL, 2016. Atypical presentation of CRB1 retinopathy. Acta Ophthalmol94, e513–514. [PubMed: 26914788]

Nadal-Nicolas FM, Kunze VP, Ball JM, Peng BT, Krishnan A, Zhou G, Dong L, Li W, 2020. True S-cones are concentrated in the ventral mouse retina and wired for color detection in the upper visual field. Elife9.

Nikonov SS, Daniele LL, Zhu X, Craft CM, Swaroop A, Pugh EN Jr., 2005. Photoreceptors of Nrl −/− mice coexpress functional S- and M-cone opsins having distinct inactivation mechanisms. J Gen Physiol125, 287–304. [PubMed: 15738050]

Nikonov SS, Kholodenko R, Lem J, Pugh EN Jr., 2006. Physiological features of the S- and M-cone photoreceptors of wild-type mice from single-cell recordings. J Gen Physiol127, 359–374. [PubMed: 16567464]

Norris P, Griffiths DW, 1983. Use of the cryostat section in electron microscopy. J Clin Pathol36, 903–906. [PubMed: 6348101]

Parry JW, Bowmaker JK, 2002. Visual pigment coexpression in Guinea pig cones: a microspectrophotometric study. Invest Ophthalmol Vis Sci43, 1662–1665. [PubMed: 11980888]

Peichl L, 2005. Diversity of mammalian photoreceptor properties: adaptations to habitat and lifestyle? Anat Rec A Discov Mol Cell Evol Biol287, 1001–1012. [PubMed: 16200646]

Reh TA, 2016. Photoreceptor Transplantation in Late Stage Retinal Degeneration. Invest Ophthalmol Vis Sci57, ORSFg1–7. [PubMed: 27116664]

Rohlich P, van Veen T, Szel A, 1994. Two different visual pigments in one retinal cone cell. Neuron13, 1159–1166. [PubMed: 7946352]

Samardzija M, Caprara C, Heynen SR, Willcox DeParis S, Meneau I, Traber G, Agca C, von Lintig J, Grimm C, 2014. A mouse model for studying cone photoreceptor pathologies. Invest Ophthalmol Vis Sci55, 5304–5313. [PubMed: 25034607]

Samson M, Emerson MM, Cepko CL, 2009. Robust marking of photoreceptor cells and pinealocytes with several reporters under control of the Crx gene. Dev Dyn238, 3218–3225. [PubMed: 19882727]

Santos-Ferreira T, Postel K, Stutzki H, Kurth T, Zeck G, Ader M, 2015. Daylight vision repair by cell transplantation. Stem Cells33, 79–90. [PubMed: 25183393]

Schaal KB, Freund KB, Litts KM, Zhang Y, Messinger JD, Curcio CA, 2015. OUTER RETINAL TUBULATION IN ADVANCED AGE-RELATED MACULAR DEGENERATION: Optical Coherence Tomographic Findings Correspond to Histology. Retina35, 1339–1350. [PubMed: 25635579]

Shelley EJ, Madigan MC, Natoli R, Penfold PL, Provis JM, 2009. Cone degeneration in aging and age-related macular degeneration. Arch Ophthalmol127, 483–492. [PubMed: 19365029]

Singh MS, Balmer J, Barnard AR, Aslam SA, Moralli D, Green CM, Barnea-Cramer A, Duncan I, MacLaren RE, 2016. Transplanted photoreceptor precursors transfer proteins to host photoreceptors by a mechanism of cytoplasmic fusion. Nat Commun7, 13537. [PubMed: 27901042]

Singh MS, Charbel Issa P, Butler R, Martin C, Lipinski DM, Sekaran S, Barnard AR, MacLaren RE, 2013. Reversal of end-stage retinal degeneration and restoration of visual function by photoreceptor transplantation. Proc Natl Acad Sci U S A110, 1101–1106. [PubMed: 23288902]

Smiley S, Nickerson PE, Comanita L, Daftarian N, El-Sehemy A, Tsai EL, Matan-Lithwick S, Yan K, Thurig S, Touahri Y, Dixit R, Aavani T, De Repentigny Y, Baker A, Tsilfidis C, Biernaskie J, Sauve Y, Schuurmans C, Kothary R, Mears AJ, Wallace VA, 2016a. Corrigendum: Establishment of a cone photoreceptor transplantation platform based on a novel cone-GFP reporter mouse line. Sci Rep6, 24012. [PubMed: 27102716]

Smiley S, Nickerson PE, Comanita L, Daftarian N, El-Sehemy A, Tsai EL, Matan-Lithwick S, Yan K, Thurig S, Touahri Y, Dixit R, Aavani T, De Repentingy Y, Baker A, Tsilfidis C, Biernaskie J, Sauve Y, Schuurmans C, Kothary R, Mears AJ, Wallace VA, 2016b. Establishment of a cone photoreceptor transplantation platform based on a novel cone-GFP reporter mouse line. Sci Rep6, 22867. [PubMed: 26965927]

Sobaci G, Ozge G, Gundogan FC, 2012. Cone dysfunctions in retinitis pigmentosa with retinal nerve fiber layer thickening. Clin Ophthalmol6, 473–478. [PubMed: 22536039]

Stuck MW, Conley SM, Naash MI, 2012. Defects in the outer limiting membrane are associated with rosette development in the Nrl−/− retina. PLoS One7, e32484. [PubMed: 22427845]

Thiadens AA, Roosing S, Collin RW, van Moll-Ramirez N, van Lith-Verhoeven JJ, van Schooneveld MJ, den Hollander AI, van den Born LI, Hoyng CB, Cremers FP, Klaver CC, 2010. Comprehensive analysis of the achromatopsia genes CNGA3 and CNGB3 in progressive cone dystrophy. Ophthalmology117, 825–830 e821. [PubMed: 20079539]

Waldron PV, Di Marco F, Kruczek K, Ribeiro J, Graca AB, Hippert C, Aghaizu ND, Kalargyrou AA, Barber AC, Grimaldi G, Duran Y, Blackford SJI, Kloc M, Goh D, Zabala Aldunate E, Sampson RD, Bainbridge JWB, Smith AJ, Gonzalez-Cordero A, Sowden JC, Ali RR, Pearson RA, 2018. Transplanted Donor- or Stem Cell-Derived Cone Photoreceptors Can Both Integrate and Undergo Material Transfer in an Environment-Dependent Manner. Stem Cell Reports10, 406–421. [PubMed: 29307580]

Wenzel A, von Lintig J, Oberhauser V, Tanimoto N, Grimm C, Seeliger MW, 2007. RPE65 is essential for the function of cone photoreceptors in NRL-deficient mice. Invest Ophthalmol Vis Sci48, 534–542. [PubMed: 17251447]

Williams GA, Jacobs GH, 2007. Cone-based vision in the aging mouse. Vision Res47, 2037–2046. [PubMed: 17509638]

Yzer S, van den Born LI, Zonneveld MN, Lopez I, Ayyagari R, Teye-Botchway L, Mota-Vieira L, Cremers FP, Koenekoop RK, 2007. Molecular and phenotypic analysis of a family with autosomal recessive cone-rod dystrophy and Stargardt disease. Mol Vis13, 1568–1572. [PubMed: 17893657]

Zhong X, Gutierrez C, Xue T, Hampton C, Vergara MN, Cao LH, Peters A, Park TS, Zambidis ET, Meyer JS, Gamm DM, Yau KW, Canto-Soler MV, 2014. Generation of three-dimensional retinal tissue with functional photoreceptors from human iPSCs. Nat Commun5, 4047. [PubMed: 24915161]

Highlights

- The *OPN1LW-EGFP/NRL*$^{-/-}$ mouse has a cone-rich retina expressing a cone-specific EGFP reporter
- *OPN1LW.EGFP* reporter expression increased the severity of the transient retinal degeneration that is typically seen in *NRL* $^{-/-}$ mice
- Donor *OPN1LW-EGFP/NRL*$^{-/-}$ cone photoreceptors differentiated into cone subtypes after long-term transplantation
- Photoreceptor sheet transplantation may promote greater macroscopic graft integrity and S-opsin+ cone survival than cell suspension transplantation

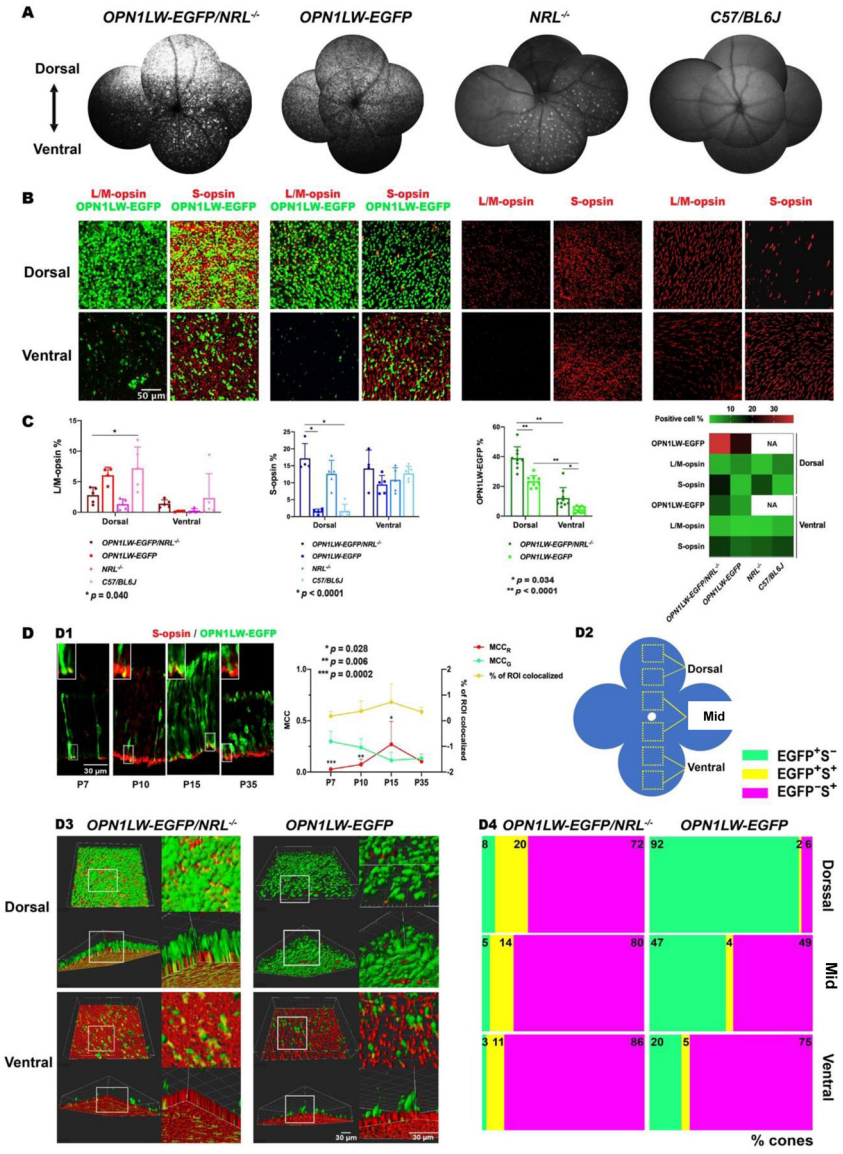

Fig. 1. Characterization of cone photoreceptors in *OPN1LW-EGFP/NRL*$^{-/-}$ mice by SWF imaging and immunohistochemistry (IHC).

(A) SWF imaging showed the density and topography of OPN1LW-EGFP^{+} photoreceptors in the fundus of *OPN1LW-EGFP/NRL*$^{-/-}$ mice and control mice (*OPN1LW-EGFP, NRL*$^{-/-}$, *C57BL/6J* mice).

(B) Retinal flat mount of *OPN1LW-EGFP/NRL*$^{-/-}$ mice (P36) and age-matched control mice were stained with L/M-opsin (L/M-cone) and S-opsin (S-cone). Anti-GFP-FITC was used to highlight OPN1LW-EGFP^{+} cells. Representative images showed the morphology and distribution of L/M- and S-cone subpopulations in both dorsal- and ventral- retina.

(C) Quantification of OPN1LW-EGFP, L/M-opsin, and S-opsin density in retinal flat-mounts of *OPN1LW-EGFP/NRL*$^{-/-}$ and control mice. The heatmap shows the density topography of cone-specific markers (OPN1LW-EGFP, L/M-opsin, S-opsin) in the strains studied.

(D) Colocalization analysis using IHC staining of GFP-FITC and S-opsin. (D1) retinal sections from *OPN1LW-EGFP/NRL*$^{-/-}$ mice (P7, P10, P15, and P35) showed the co-

localization of S-opsin and OPN1LW-EGFP expression (magnified in the upper left corner of each panel). Co-localization frequency of S-opsin and OPN1LW-EGFP was quantified by % of ROI colocalized. Fractions of OPN1LW-EGFP and S-opsin signal in colocalized compartments were analyzed via MCC (MCC_G and $MCC_{R,}$ respectively); (D2) Schematic presenting the imaging regions of interest (ROIs) on retinal flat mounts from *OPN1LW-EGFP/NRL*$^{-/-}$ and *OPN1LW-EGFP* mice (P35); (D3) Representative 3D-images showed the colocalization of OPN1LW-EGFP and S-opsin on retina flat mounts (magnified on the right for each panel); (D4) Spots colocalization counting of % cones that co-expressed OPN1LW-EGFP and S-opsin ($EGFP^+S^+$), or purely expressed OPN1LW-EGFP ($EGFP^+S^-$) or S-opsin ($EGFP^-S^+$). *Abbreviations: SWF: short-wavelength fluorescence; ROI: region of interest; MCC: Mander's colocalization coefficient.*

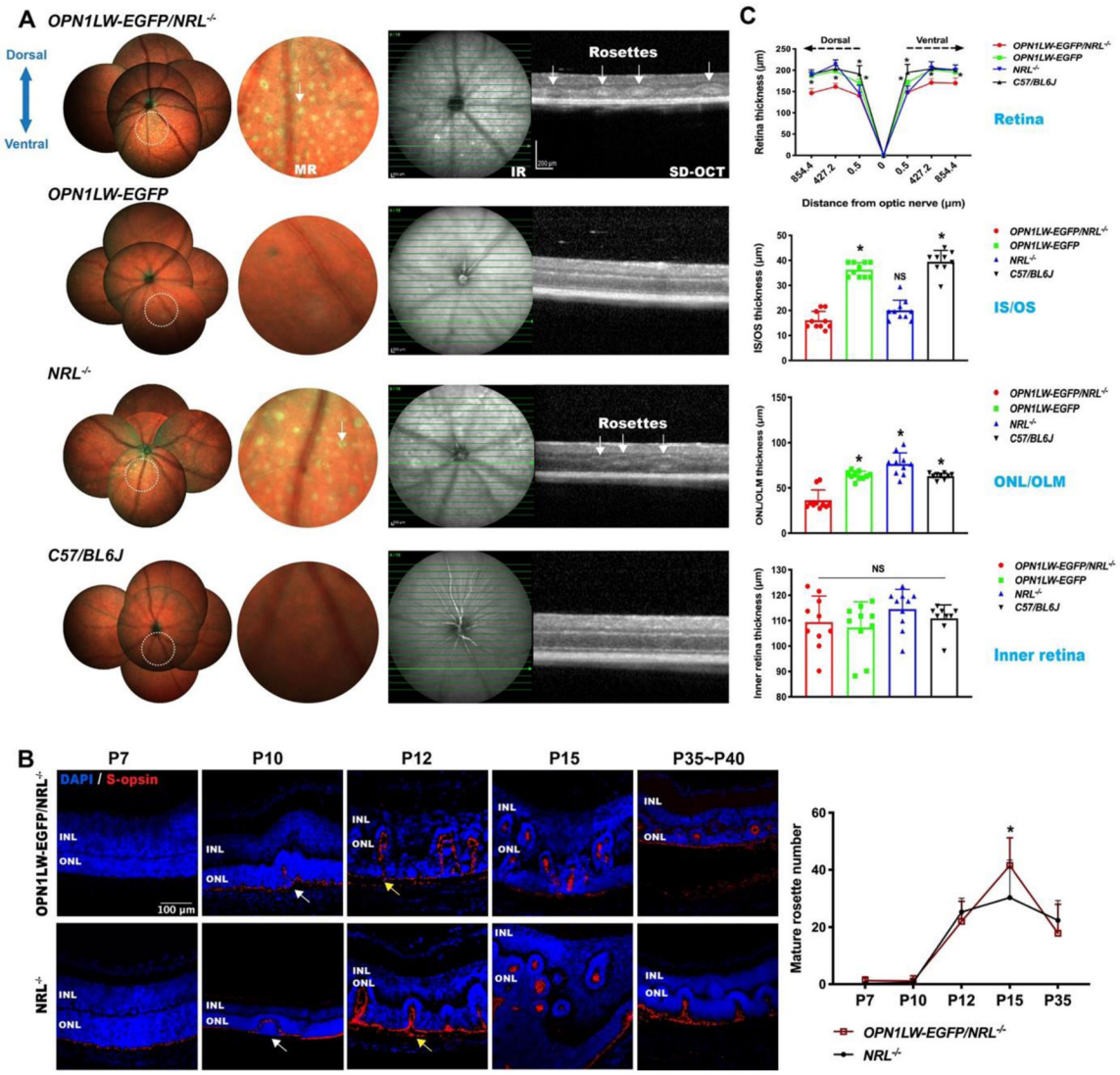

Fig. 2. Rosette development and retinal thinning in *OPN1LW-EGFP/NRL*$^{-/-}$ mice.

(A) MR imaging and SD-OCT scanning of *OPN1LW-EGFP/NRL*$^{-/-}$, *OPN1LW-EGFP, NRL*$^{-/-}$, and *C57BL/6J* (wild-type) mice. White arrows: representative rosettes.

(B) Retina sections stained with S-opsin showed rosette development in *OPN1LW-EGFP/NRL*$^{-/-}$ and *NRL*$^{-/-}$ mice (from P7 to P35~P40). There were comparable numbers of mature rosettes in the *OPN1LW-EGFP/NRL*$^{-/-}$ and *NRL*$^{-/-}$ mice during development, except for at P15 where the number of rosettes in *OPN1LW-EGFP/NRL*$^{-/-}$ were higher (*p = 0.015). Data were collected from both the dorsal and the ventral retina. White arrows: representative nascent rosettes; Yellow arrows: representative mature rosettes.

(C) Whole retina thickness was computed on SD-OCT B-scans across the different retinal regions (0.5 μm, 427.2 μm, and 854.4 μm from the optic nerve). The thickness of photoreceptor inner and outer segments (IS/OS), the outer retina (ONL/OLM), and the inner retina (OPL, INL, IPL, RGC) were quantified at a distance of 427.2 μm in the dorsal retina. * $p < 0.0001$.

Abbreviations: MR: multicolor reflectance; IR: infrared; SD-OCT: spectral domain optical coherence tomography; INL: inner nuclear layer; ONL: outer nuclear layer.

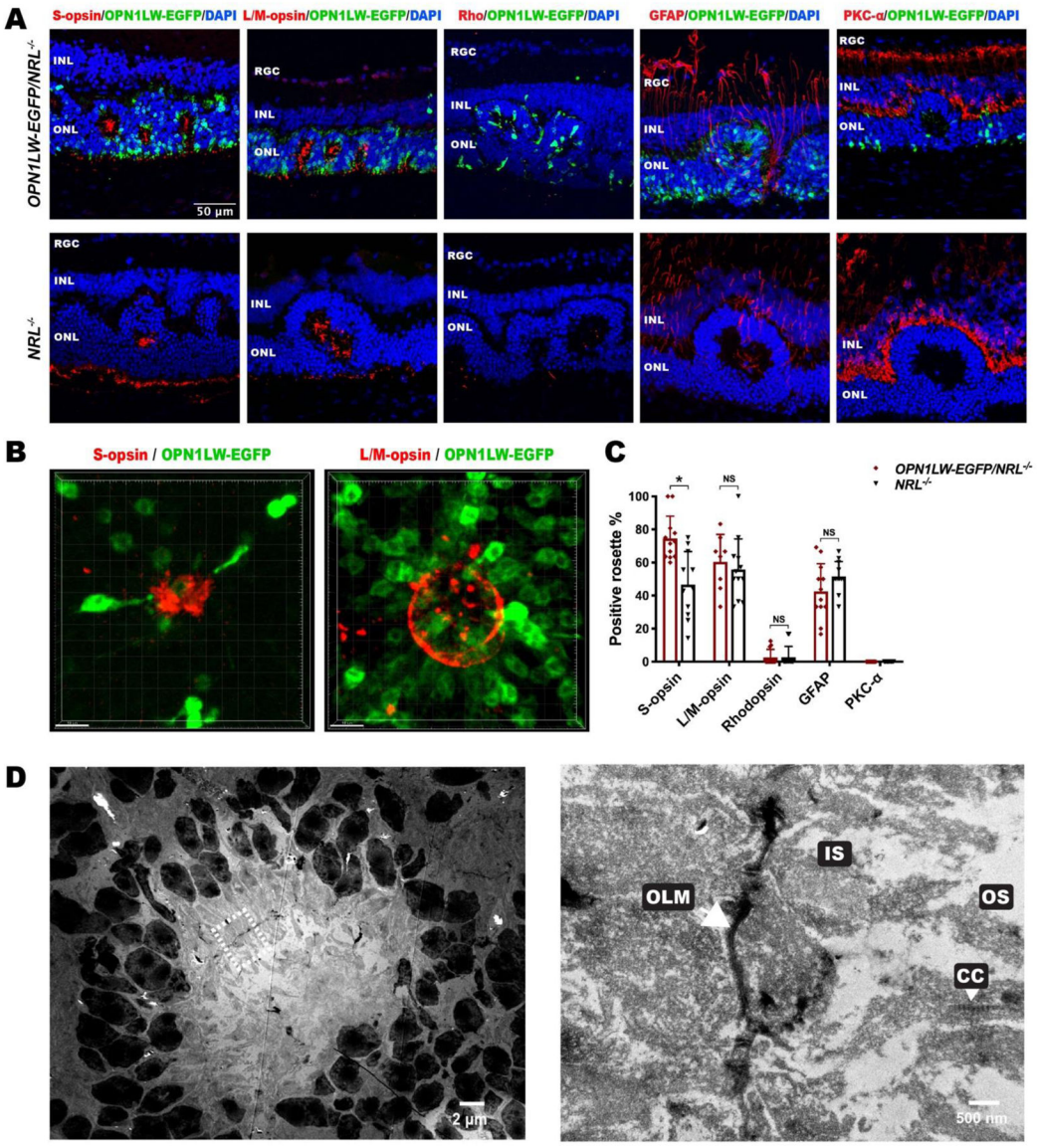

Fig. 3. Cellular composition of rosettes in *OPN1LW-EGFP/NRL*$^{-/-}$ mice.

(A) IHC images of P35 *OPN1LW-EGFP/NRL*$^{-/-}$ retinal sections stained with retinal specific markers, including S-opsin, L/M-opsin, Rhodopsin, GFAP, and PKC-α, with age-matched *NRL*$^{-/-}$ retina as control.

(B) Three-dimensional reconstitution of S-opsin^{+} and L/M-opsin^{+} rosette on retina flat mount of *OPN1LW-EGFP/NRL*$^{-/-}$ mice (P35).

(C) Quantification of rosettes that were positive for each marker in *OPN1LW-EGFP/NRL*$^{-/-}$ and *NRL*$^{-/-}$ mice. * $p < 0.0001$. NS: not significant.

(D) Transmission electron microscopy of a representative rosette in *OPN1LW-EGFP/NRL*$^{-/-}$ mice (P35). The magnified image is on the right side.

Abbreviations: RGC: retinal ganglion cell; INL: inner nuclear layer; ONL: outer nuclear layer; OLM: outer limiting membrane; IS: inner segment; CC: connecting cilium; OS: outer segment.

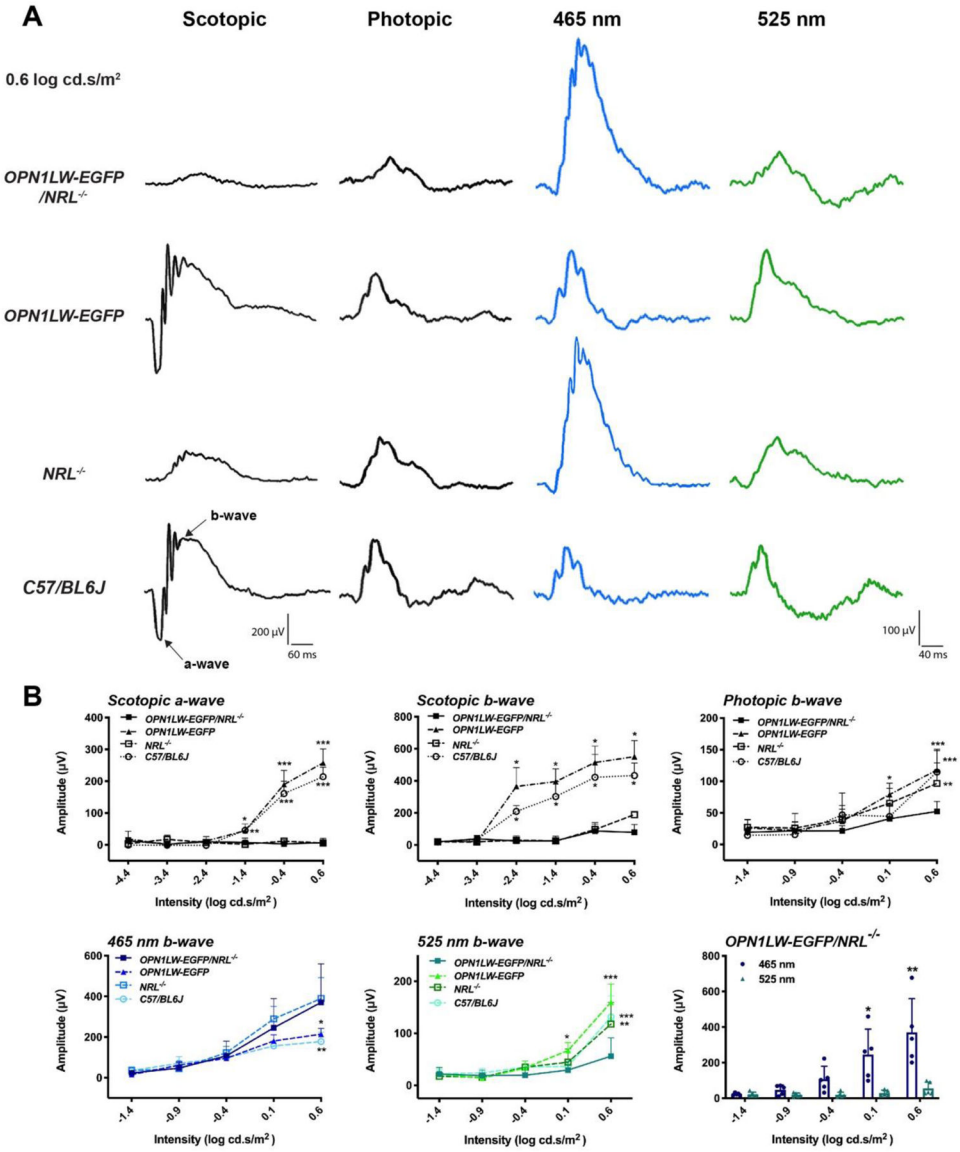

Fig. 4. Retinal function tested by full-field electroretinography (ERG).

(A) Representative ERG responses of *OPN1LW-EGFP/NRL*$^{-/-}$ mice and control mice (*OPN1LW-EGFP, NRL*$^{-/-}$*, C57BL/6J* mice). Scotopic-, photopic-, 465 nm-, and 525 nm-stimuli ERG were performed to evaluate the function of rods, cones, S-cones, and M-cones, respectively. All waveforms start at 0 millisecond (ms). Stimulus intensity was 0.6 log cd.s/m^2 in each case.

(B) Comparison of the full-field ERG response amplitudes between *OPN1LW-EGFP/NRL*$^{-/-}$ and control mice over an intensity response range.

Statistical analysis:

Scotopic a-wave: * $p = 0.016$ (*OPN1LW-EGFP/NRL*$^{-/-}$ vs *C57BL/6J*), ** $p = 0.021$(*OPN1LW-EGFP/NRL*$^{-/-}$ vs *OPN1LW-EGFP*), *** $p < 0.0001$.

Scotopic b-wave: * $p < 0.0001$.

Photopic b-wave: * $p = 0.028$, ** $p = 0.008$, *** $p < 0.0001$.

465 nm stimuli b-wave: * $p = 0.002$, ** $p < 0.0001$.
525 nm stimuli b-wave: * $p = 0.035$, ** $p = 0.0001$, *** $p < 0.0001$.
Comparison of 465 nm and 525 nm b-wave amplitude in OPN1LW-EGFP/NRL$^{-/-}$ mice: * $p = 0.0006$, ** $p < 0.0001$.

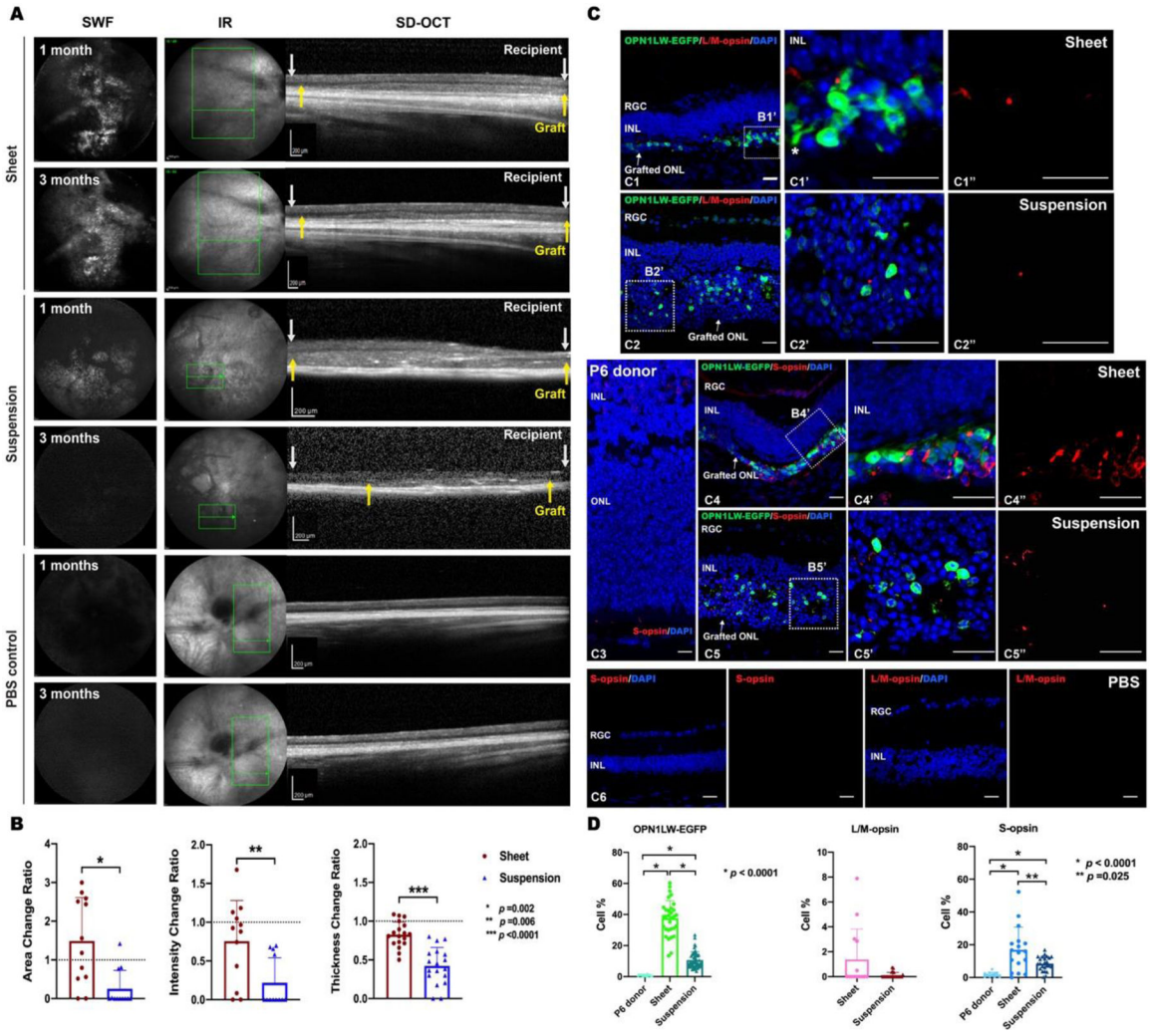

Fig. 5. Evaluation of grafted *OPN1LW-EGFP/NRL*$^{-/-}$ retinal suspensions and sheet grafts in *Rd1/NS* recipients.

(A) Multimodal cSLO images from representative *Rd1/NS* recipients and PBS mock transplanted *Rd1/NS* control mice. SWF and SD-OCT imaging were used to track the grafted retinal sheet and suspension from *OPN1LW-EGFP/NRL*$^{-/-}$ mice at 1 month and 3 months post-transplantation. Between white arrows: recipient retina; Between yellow arrows: retina grafts.

(B) The mean change ratios of graft area and intensity from 1 month to 3 months were compared between sheet and suspension grafts on SWF imaging. The mean thickness change ratio of sheet and suspension grafts over three months was quantified on SD-OCT images. For sheet versus suspension grafts: Area change ratio: 1.49 ± 1.12 vs. 0.25 ± 0.48, n =12, p =0.002; Intensity change ratio: 0.76 ± 0.53 vs. 0.21 ± 0.32, n =12, p = 0.006; Thickness change ratio: 0.92 ± 0.12 vs. 0.42 ± 0.30, n =18, p <0.0001.

(C) IHC staining of OPN1LW-EGFP and cone-specific markers (L/M-opsin, S-opsin) was performed on sheet and suspension grafts (C1–C2, C4–C5)), and PBS-transplanted controls (C6), at 3 months post-transplantation and P6 *OPN1LW-EGFP/NRL*$^{-/-}$ donor retina controls (C3). Asterisk: neurite of a grafted cone photoreceptor. Scale bar = 20 μm.

(D) Quantification of grafted cone subpopulations expressing OPN1LW-EGFP, L/M-opsin, and S-opsin in retinal sheet graft, suspension graft, and the P6 *OPN1LW-EGFP/NRL*$^{-/-}$ donor retina sections.

Abbreviations: SWF: short-wavelength fluorescence; MR: multicolor reflectance; IR: infrared; SD-OCT: spectral domain optical coherence tomography; RGC: retinal ganglion cell; INL: inner nuclear layer.